ISSN 1392 - 1207. MECHANIKA. 2012 Volume 18(5): 534-538

Numerical study of elliptic and coaxial jets with variable density

M. Senouci*, M. Belkadi, B. Bouguenina***, B. Imine******
**Mechanical Engineering Faculty, UST Oran, B.P 1505 El Mnaouer U.S.T. Oran. Algeria,*
E-mail: senoucimahi@yahoo.fr
***Mechanical Engineering Faculty, USTO Oran, B.P 1505 El Mnaouer U.S.T. Oran, Algeria, E-mail: mbelkadi@yahoo.fr*
****School Doctorate SNEF USTO Oran, B.P 1505 El Mnaouer U.S.T. Oran, Algeria, E-mail: 6609011984@hotmail.com*
*****Aeronautical Laboratory and Propulsive Systems, USTO Oran, B.P 1505 El Mnaouer U.S.T. Oran, Algeria,*
E-mail: imine_b@yahoo.fr

crossref http://dx.doi.org/10.5755/j01.mech.18.5.2693

Nomenclature

D - nozzle diameter, mm; D_a - co-flowing diameter, mm; $D_{eq} = D_e$ - equivalent diameter of elliptic nozzle, mm; F_c - mass fraction; L_p - potential core length from density field; L_a - co-flowing length, mm; M - outer to inner specific momentum flux ratio; R_v - outer to inner bulk velocity ratio; S - outer to inner density ratio; U - jet exit mean velocity, m/s; U_a - co-flowing velocity, m/s; X - distance to nozzle, m; ρ - density: ρ^* normalized density = $(\rho-\rho_e)/(\rho_i-\rho_e)$ or $(\rho-\rho_{He})/(\rho_i-\rho_{He})$; $(-)_i$ - relative to inner jet; $(-)_e$ - relative to external jet; $(-)_a$ - relative to ambient fluid.

1. Introduction

The coaxial turbulent jets with variable density form a fluid mechanical problem encountered in several applications (propulsion, combustion). A coaxial configuration as shown in Fig. 1 consists of two coaxial nozzle diameters D_e and D_i and opening into an enclosure. This dual nozzle carries two fluids air and helium, the first in the central nozzle with velocity U_i and density ρ_i, the other flowing through the annular space with velocity U_e and density ρ_e. The two fluids transported by the double nozzle are injected into a stagnant environment. The injection systems used in many combustion chambers of rocket engine, turbine engine and industrial burners are coaxial jets because they provide high mixing performance. These flows are characterized by a sharp variation in density mainly due to mixing of different fluids but also possibly due to compressibility effects or temperature variation. The quality of the resulting mixture through coaxial jets is the result of a series of complex physical phenomena occurring in the initial zone. These phenomena are essentially a transition to turbulence; they depend heavily on conditions at the entrance. Thus acting through physical or geometric parameters of the entrance, we can control the flow.

The first experimental studies on coaxial jets went back to the post World War II. In a series of work, Ko et al. [1-3] investigated the area close to a homogeneous and isothermal coaxial jets for speed ratios. The study of Gladnick and al. [4] allowed show the influence of velocity ratio on the mixing performance of coaxial heterogeneous jets. The central jet consisting of CFC-12 and the annular jet of air, and the velocity ratio ranging from 0.26 to 2. The increase in the velocity ratio promotes mixing by penetration of the central jet.

On the numerical tier, heterogeneous coaxial jets have been studied by Ghia and al. [5] for a velocity ratio greater than one and different density ratio; he concluded that mixing is favored when the transverse gradients of density and velocity are opposites. This configuration is encountered in the case of engines seminated where oxygen is in the center and hydrogen in the ring, and where the ejection velocity of hydrogen is higher than that of oxygen. Harran [6] simulated coaxial jets of hydrogen and air using second-order modeling. It was also used static decompositions that lead to different variations on the mean and turbulent sizes. Guenoune [7] simulated a coaxial jets corresponding to the experimental work carried out by Favre-Marinet et al [8] by using Favre average and the model k-epsilon. It was inferred that the numerical simulation gives a good result. In the work of Favre-Marinet et al [9], an experimental study of the density field of coaxial jets with large density differences is investigated. The density field was determined by a thermo-anemometric method based on a new version of an aspirating probe. However, measurement shown that mixing is directly dependent upon the flow dynamics in the near field region.

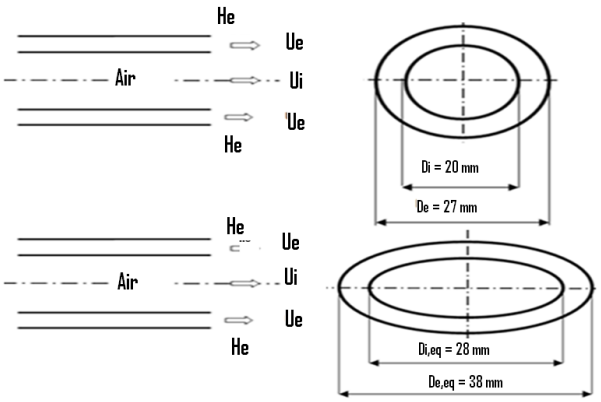

Fig. 1 Schemes of a circular and elliptic coaxial configuration

This work is a part of an effort to provide a contribution to the study of the influence of the shape of the nozzle of coaxial jets on mixing performance. The modified geometry is a technical control called passive promising and will be tested in this work. It is thus suggested to replace the circular shape of the nozzle by an equivalent elliptical shape. The coaxial jets are produced through circular and elliptic nozzles. The elliptic and circular nozzles have approximately the same exit area. The objective of this work is to predict by numerical simulation the influence of the elliptical shape of the injection section on

the performance of a mixture of coaxial jets. To do a validation of this work with experiment, it was based on the experimental work of Favre-Martinet et al. [9]. The same operating conditions have been adopted.

2. Conservation equations and turbulence models

In the mathematical description of the conservation equations, all variables, except the pressure and the density, which are always computed according to Reynolds average, are Favre [10] average (mass-weighted). This quantity is defined as

$$\tilde{\Phi} = \frac{\overline{\rho \Phi}}{\bar{\rho}} \tag{1}$$

The asymmetric turbulent jet with variable density is a monophasic and 3D flow of Newtonian fluid, which can be regarded as a perfect gas. The general form for the transport equations as follows:

1. Average equation of the continuity

$$\frac{\partial}{\partial x_j}\left(\bar{\rho}\tilde{U}_j\right) = 0 \tag{2}$$

2. Average equation of the momentum conservation

$$\frac{\partial}{\partial x_j}\left(\bar{\rho}\tilde{U}_i\tilde{U}_j\right) = \bar{\rho}g_i - \frac{\partial \bar{p}}{\partial x_i} - \frac{\partial}{\partial x_j}\left(\overline{\rho u_i'' u_j''}\right) + \\ + \frac{\partial}{\partial x_j}\left[\bar{\mu}\left(\frac{\partial \tilde{U}_i}{\partial x_j} + \frac{\partial \tilde{U}_j}{\partial x_i}\right) - \frac{2}{3}\bar{\mu}\frac{\partial \tilde{U}_k}{\partial x_k}\delta_{ij}\right] \tag{3}$$

3. Average equation of the mixture fraction conservation

$$\frac{\partial}{\partial x_j}\left(\bar{\rho}\tilde{F}\tilde{U}_j\right) = -\frac{\partial \bar{d}_j^k}{\partial x_j} - \frac{\partial}{\partial x_j}\left(\overline{\rho f'' u_j''}\right) \tag{4}$$

$$\bar{d}_j^k = -\frac{\lambda}{C_p}\frac{\partial \tilde{F}}{\partial x_j} \tag{5}$$

The mean density can be obtained from the mean mixture fraction using the equation of state. With constant pressure, this leads to

$$\frac{1}{\bar{\rho}} = \frac{F}{\rho_j} + \frac{1-F}{\rho_a} \tag{6}$$

4. The Reynolds stress model (RSM)

The Reynolds stresses $\overline{\rho u''u''}$, $\overline{\rho v''v''}$, $\overline{\rho w''w''}$ and $\overline{\rho u''v''}$ may be written as follows

$$\frac{\partial}{\partial x_k}\left(\tilde{U}_k\,\overline{\rho u_i'' u_j''}\right) = P_{ij} + G_{ij} + D_{ij} + \\ + \overline{p'\left(\frac{\partial u_i''}{\partial x_j} + \frac{\partial u_j''}{\partial x_i}\right)} - \frac{2}{3}\bar{\rho}\varepsilon\delta_{ij} \tag{7}$$

where, the assumption of the isotropy for the smallest scales has been assumed.

$$P_{ij}, G_{ij}, D_{ij} \quad \text{and} \quad \overline{p'\left(\frac{\partial u_i''}{\partial x_j} + \frac{\partial u_j''}{\partial x_i}\right)} \tag{8}$$

The first term is the production term due the mean strain

$$P_{ij} = -\left(\overline{\rho u_i'' u_k''}\right)\frac{\partial \tilde{U}_j}{\partial x_k} - \left(\overline{\rho u_j'' u_k''}\right)\frac{\partial \tilde{U}_i}{\partial x_k} \tag{9}$$

While the second term is the production due the buoyancy effects

$$G_{ij} = -\beta\left(g_i\,\overline{\rho u_j'' f''} + g_j\,\overline{\rho u_i'' f''}\right) \tag{10}$$

And the diffusion term is modelled as

$$D_{ij} = C_s\frac{\partial}{\partial x_k}\left[\left(\frac{k}{\varepsilon}\left(\overline{\rho u_k'' u_l''}\right) + \bar{\rho}\delta_{kl}\nu\right)\frac{\partial\left(\overline{\rho u_i'' u_j''}\right)}{\partial x_l}\right] \tag{11}$$

where, the turbulent kinetic energy is defined as

$$k = \frac{1}{2}\overline{u''_i\,u''_i} \tag{12}$$

The dissipation rate equation is exactly the same as in the standard $k-\varepsilon$ model and has the form

$$\frac{\partial}{\partial x_k}\left(\rho\tilde{U}_k\varepsilon\right) = \frac{\varepsilon}{k}\left(C_{\varepsilon 1}P - C_{\varepsilon 2}\rho\varepsilon\right) + \frac{\partial}{\partial x_k}\left[\left(\mu + \frac{\mu_t}{\sigma_\varepsilon}\right)\frac{\partial \varepsilon}{\partial x_k}\right] \tag{13}$$

One can find more details concerning modelling of the Reynolds stress equations and their constants in reference [11].

3. Boundary conditions

In the case of elliptic coaxial jets and for the reasons of symmetry, only the quarter of the physical field is considered as computational domain with the following considerations: at the inlet, and in order to overcome as much as possible the influence of the jet and the co-flow emissions [11], the velocity, the Reynolds stresses and the turbulent kinetic energy profiles were calculated by extrapolating the measured values at $X/D_{eq} = 0.3$. The lateral and the transverse velocities and scalar variance are zero. The mixture fraction is one at the inlet jet and zero at inlet co-flowing.

4. Numerical method

The equations describing a confined turbulent flow are of elliptic convection-diffusion. These equations are solved by a finite volume method as described by Patankar [12] and Benhamza [13]. For the numerical solution of these equations a computer code was developed. The terms of the differential on the volume interfaces are obtained by a second order upwind scheme. The pressure velocity coupling is achieved by the SIMPLE algorithm of

Patankar and Spalding [12]. The grid extends gradually in all directions in order to take into account of the jet development in the co-flowing. Four grid sizes (40×40×80, 50×50×80, 60×60×120 and 70×70×120 mm) have been tested for the grid independency of the solution for elliptic and rectangular nozzles. The results are independent of numerical influences for grids finer than the 60×60×120 mesh. Thus the calculation of an asymmetrical jet requires, on average, nine hours and twenty minutes of CPU time on a Pentium 4 computer.

5. Results and discussions

The elliptic and circular coaxial jets of binary mixture of He-air, with a momentum aspect ratio M are investigated in the present study. The elliptic nozzle has approximately the same exit area as the circular nozzle. The inner and outer jets have two equivalent diameters D_e = 27 mm and D_i = 20 mm, and are injected at atmospheric pressure and inlet velocity U_e = 16 m/s and $U_i = U_e/R_v$ with $3 < R_v < 70$. For all calculations, the studied jets are considered slightly confined and the co-flowing is considered cylindrical with a diameter D_a = 300 mm and a length L_a = 1000 mm. The co-flowing is injected with a velocity U_a = 0.01 m/s at the same pressure condition as the jet. The co-flow inlet velocity is chosen so that it prevents the presence of recirculation zones. This problem is normally avoided when the Craya-Curtet parameter [14] for variable density flows is maintained above 0.8, irrespective of the fluid considered. The geometric parameters and the inlet velocities used in the present computation are the same as those in the experimental work of Favre-Martinet et al. Table [9].

Table

Operating conditions of Favre-Martinet

M	R_v	U_i, m/s
1.0	4	4
4.0	5.38	2.97
9.0	8.08	1.98
36.0	16.15	0.99

5.1. Density

Figs. 2-5 shows the evolution of the normalized density to the jet axis for different momentum ratios M. In each figure the experimental and numerical results of circular and elliptical cases are grouped.

According to Fig. 2 the numerical results of density normalized of circular case shows a plateau value of unity to an abscissa X/D_i = 4.0, then decreases to a value equal to ρ^* = 0.45 to abscissa X/D_i = 20 and finally it stabilizes. The experimental measurements on the other hand show that the level of unit value extends beyond the bearing of numerical results up to X/D_i = 5.0 and then decreases with a slope comparable to the curve of numerical results to reach a minimum value ρ* equal to 0.6 corresponding to an abscissa X/D_i = 10 and then rises.

The numerical results of the elliptical case show that the normalized density decreases rapidly to reach a minimum of ρ^* equal to 0.6 abscissa X/D_i = 5.0 and then rises.

The numerical results of the circular case and experimental measurements are similar for lower abscissa X/D_i = 2.0. The numerical profile decreases more rapidly than the experimental profile to a value below the minimum of experimental measurements and stabilizes. And experimental results are validated to X/D_i = 10.0 beyond this distance the experimental results and numerical results do not match. That is due to the low number of sowing particles at the nozzle edges and far from its emission section making experimental measurements difficult and consequently inaccurate.

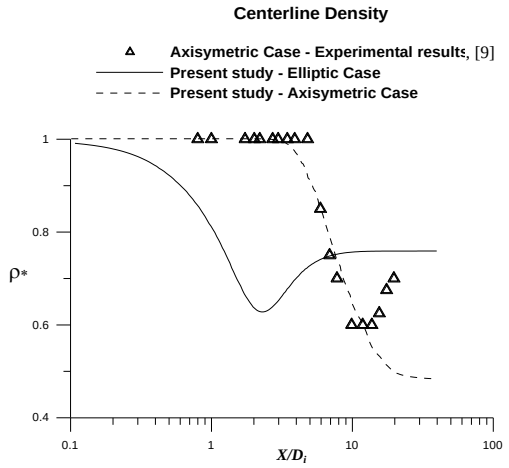

Fig. 2 Validation of axial density profile, M = 1

Differences between the elliptic coaxial jets studied and the circular coaxial jets are observed for the normalized density distribution. The comparison of numerical results of the case of circular and elliptical cases shows that the decrease in the density of elliptic case starts faster than the circular case. In addition to the minimum density of the elliptic case and the circular case are different. One can notice that the mixing between the elliptic coaxial jets and the co-flowing is carried out more rapidly in this type of jet than in a circular one.

For M = 4 the numerical results of circular case are validated to X/D_i = 6.0. The length of cone potential of circular case L_p is of 2.0 and the minimum of normalized density is 0.4. On the other hand, in the elliptic case, the normalized density decreases rapidly to reach a minimum of 0.6.

For M = 9 case of the numerical results of circular case are validated to circular X/D_i = 3.0. The length of the

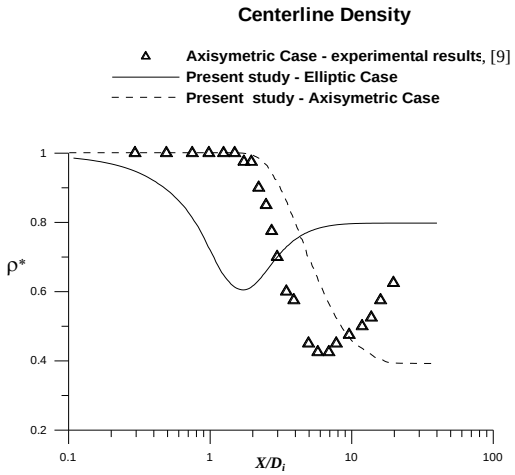

Fig. 3 Validation of axial density profile, M = 4

circular cone potential case L_p is 1.5 and according to the minimum of experimental normalized density is 0.3. On the other hand, in the elliptic case, the normalized density decreases rapidly to reach a minimum of 0.45.

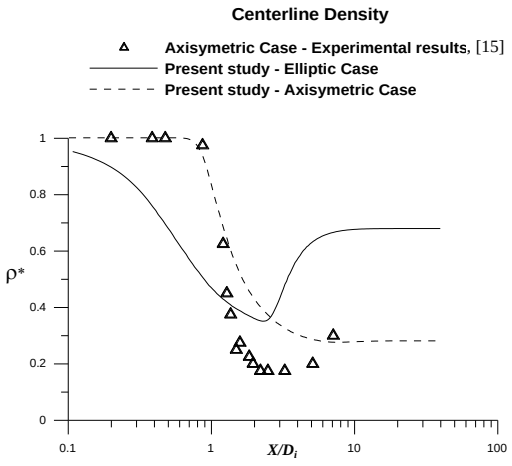

Fig. 4 Validation of the axial density profile, M = 36

For M = 36 the numerical results of circular case are validated to X/D_i = 2.0. The length of the circular cone of potential case L_p is of 0.7 and according to the experimental results of the minimum of normalized density is of 0.2 approximately. On the other hand, in the elliptic case, the normalized density decreases rapidly to reach a minimum of 0.38.

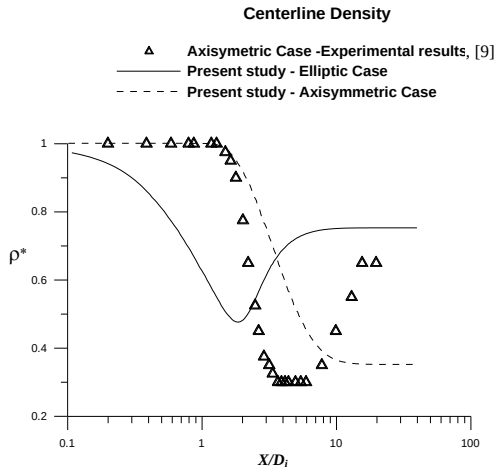

Fig. 5 Validation of the axial density profile, M = 9

The numerical results of the circular case and experimental measurements follow a similar pace until the experimental results reach a minimum after which there is divergence. The decrease in the density of the elliptic case always starts faster than the circular case. The minimum of the circular case is more important than the minimum of the elliptic case. The difference increases with increasing the ratio characteristic of momentum.

5.2. Mass fraction

Figs. 6-9 shows the characteristics for different ratios of momentum, the mass fractions of elliptical and circular according to the x-axis. All these curves look the same, and the mass fraction of Helium begins as zero, reaches a maximum and then stabilizes (or decreases). In addition, the maximum mass fraction of Helium is the minimum density dimensionless. Helium injected by the nozzle ring and enters the air and decreases the density.

For M = 1 the maximum mass fraction of Helium is of 0.10 for the elliptic case and of 0.17 for the circular case.

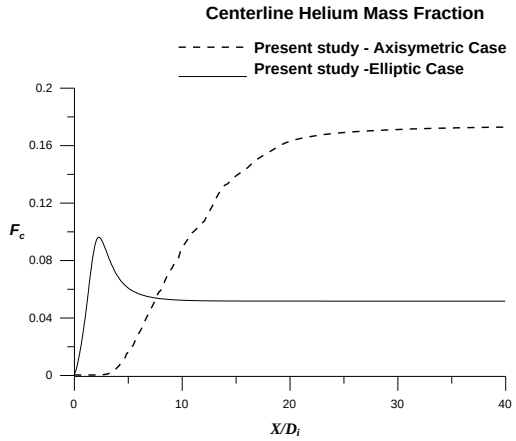

Fig. 6 Profile of mass fraction of Helium M = 1

For M = 4 the maximum mass fraction of Helium is of 0.15 for the elliptic case and of 0.25 for the circular case.

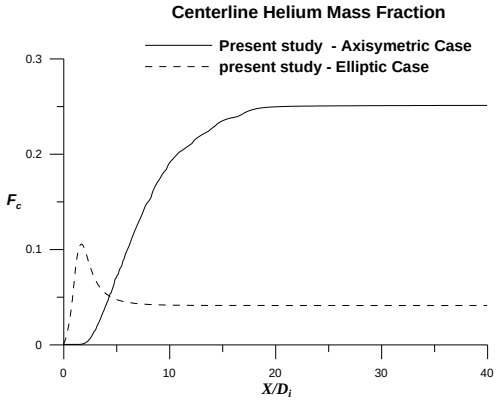

Fig. 7 Profile of mass fraction of Helium M = 4

For M = 9 for the maximum mass fraction of Helium is of 0.2 for the elliptic case and of 0.3 for the circular case.

For M = 36, the maximum mass fraction of Helium is of 0.3 for the elliptic case and of 0.4 for the circular case.

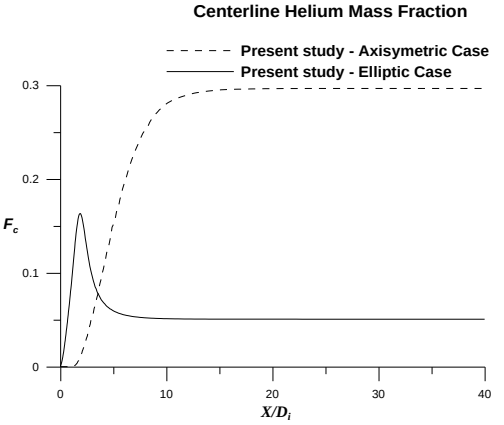

Fig. 8 Profile of mass fraction of Helium M = 9

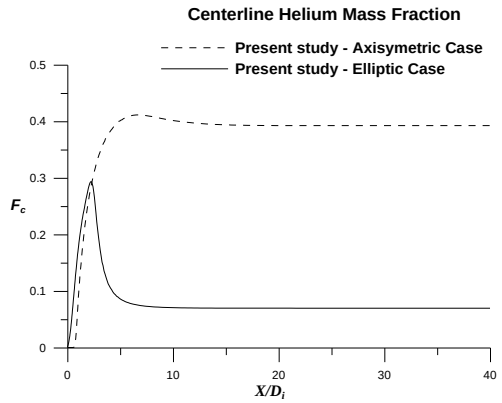

Fig. 9 Profile of mass fraction of Helium $M = 36$

6. Conclusion

The influence of nozzle geometries on a coaxial turbulent binary gas mixing asymmetric jets has been numerically investigated using a second-order Reynolds stress model (RSM). An examination of the centerline values of longitudinal normalized density and mass fraction has been presented. The prediction of the present calculation agrees reasonably well with the very recent experimental study. However, the variables calculated showed that the performances of the elliptic geometries are much higher than those of the circular. In general, the asymmetrical coaxial nozzles enhance strongly the mixing.

References

1. **Ko, N.W.M.; Kwan, A.S.H.** 1976. The initial region of subsonic coaxial jets, J. Fluid Mech. 73: 305-332. http://dx.doi.org/10.1017/S0022112076001389.
2. **Ko, N.W.M.; Au, H.** 1985. Coaxial jets of different mean velocity ratios, J. Sound and Vibration 100: 211-232. http://dx.doi.org/10.1016/0022-460X(85)90416-X.
3. **Au, H.; Ko, N.W.M.** 1987. Coaxial jets of different mean velocity ratios: Part 2, J. Sound and Vibration 116: 427-443. http://dx.doi.org/10.1016/S0022-460X(87)81375-5.
4. **Gladnick, P.; Enotiadis, J.; LaRue, J.; Samuelsen, G.** 1990. Near-field characteristics of a turbulent coflowing jet, AIAA J. 288: 1405-1414. http://dx.doi.org/10.2514/3.25232.
5. **Ghia, K.N.; Lavan, Z.; Torda, T.P.** 1968. Laminar mixing of heterogeneous axisymmetric coaxial confined jets, Final report NASA-CR-72480.
6. **Harran, G. ; Chassaing, P. ; Joly, L. ; Chibat, M.** 1996. Etude numérique des effets de densité dans un jet de mélange turbulent en microgravité, Revue Générale de Thermique 35(411): 151-176. http://dx.doi.org/10.1016/S0035-3159(96)80026-2.
7. **Guenoune, R.** 2009. Simulation numérique d'un jet coaxial turbulent avec différence de densité, Thesis of Master, Batna university, Algeria.
8. **Favre-Marinet, M.; Camano, E.; Sarboch, J.** 1999. Near-field of coaxial jets with large density differences, Exp. Fluids 26: 97-106. http://dx.doi.org/10.1007/s003480050268.
9. **Favre-Marinet, M.; Camano, E.** 2001. The density field of coaxial jets with large velocity ratio and large density differences, I. J Heat and Mass Transfer 44: 1913-1924. http://dx.doi.org/10.1016/S0017-9310(00)00240-4.
10. **Imine, B.; Imine, O.; Abidat, M.; Liazid, A.** 2006. Study of non-reactive isothermal turbulent asymmetric jet with variable density, Computational Mechanical, Springer-Verlag, 38(2): 151-162.
11. **Sanders, J.P.; Sarh, B.; Gokalp, I.** 1997. Variable density effects in axisymmetric isothermal turbulent jet: a comparison between a first and a second order turbulence model, Int. J Heat Mass Trans.40(4): 823-842. http://dx.doi.org/10.1016/0017-9310(96)00151-2.
12. **Patankar, S.V.; Spalding, D.B.** 1970. Heat and Mass Transfer in Boundary Layers, Intertext, London.
13. **Benhamza, M.E.; Belaid, F.** 2009. Computation of turbulent channel flow with variable spacing riblets, Mechanika 5(79): 36-41.
14. **Curtet, R.** 1957. Contribution à l'étude théorique des jets de révolution, Extrait des comptes rendus de l'académie des sciences 244: 1450-1453.

M. Senouci, M. Belkadi, B. Bouguenina, B. Imine

ELIPSĖS FORMOS IR BENDRAAŠIŲ KINTAMO TANKIO SRAUTŲ SKAITMENINĖ ANALIZĖ

R e z i u m ė

Šioje studijoje skaitiniu būdu ištirta elipsės formos ir bendraašių, labai skirtingo tankio įėjimo srautų geometrijos įtaka sumaišymo procesui. Bendraašiai srautai nukreipiami apvaliais ir elipsės formos antgaliais. Šių antgalių skerspjūvio plotai panašūs. Antros eilės Reinoldso įtempių modelis (RĮM) naudojamas efektams skirtingo tankio bendraašiuose turbulentiniuose srautuose įvertinti. Pateikti šių kintamųjų lyginamieji skaičiavimai. Rezultatai rodo, kad elipsės formos bendraašės geometrijos srautų sumaišymo procesas vyksta daug sparčiau negu apvalios formos srautų.

M. Senouci, M. Belkadi, B. Bouguenina, B. Imine

NUMERICAL STUDY OF ELLIPTIC AND COAXIAL JETS WITH VARIABLE DENSITY

S u m m a r y

In the present study, the effects of inlet elliptic and coaxial jet geometry on the mixing process with large density differences has been investigated numerically. The coaxial jets are produced through circular and elliptic nozzles. The elliptic and circular nozzles have approximately the same exit area. A second-order Reynolds stress model (RSM) is used to investigate variable density effects in coaxial turbulent jets. Comparative studies are presented for the calculations of the variables. The results indicate that the elliptic coaxial geometry noticeably enhances mixing in comparison with the circular case.

Keywords: numerical study, elliptic and coaxial jets, variable density.

Received March 18, 2011
Accepted September 21, 2012